



Viral 3CL^{pro} as a Target for Antiviral Intervention Using Milk-Derived Bioactive Peptides

Yasaman Behzadipour¹ · Maryam Gholampour² · Somayeh Pirhadi³ · Hassan Seradj⁴ · Mehdi Khoshneviszadeh⁴ · Shiva Hemmati^{1,2,5}

Accepted: 8 September 2021 / Published online: 16 September 2021
© The Author(s), under exclusive licence to Springer Nature B.V. 2021

Abstract

Viruses of the picornavirus-like supercluster mainly achieve cleavage of polyproteins into mature proteins through viral 3-chymotrypsin proteases (3C^{pro}) or 3-chymotrypsin-like proteases (3CL^{pro}). Due to the essential role in processing viral polyproteins, 3C^{pro}/3CL^{pro} is a drug target for treating viral infections. The 3CL^{pro} is considered the main protease (M^{pro}) of coronaviruses. In the current study, the SARS-CoV-2 M^{pro} inhibitory activity of di- and tri-peptides (DTPs) resulted from the proteolysis of bovine milk proteins was evaluated. A set of 326 DTPs were obtained from virtual digestion of bovine milk major proteins. The resulted DTPs were screened using molecular docking. Twenty peptides (**P1–P20**) showed the best binding energies ($\Delta G_b < -7.0$ kcal/mol). Among these 20 peptides, the top five ligands, namely **P1** (RVY), **P3** (QSW), **P17** (DAY), **P18** (QSA), and **P20** (RNA), based on the highest binding affinity and the highest number of interactions with residues in the active site of M^{pro} were selected for further characterization by ADME/Tox analyses. For further validation of our results, molecular dynamics simulation was carried out for **P3** as one of the most favorable candidates for up to 100 ns. In comparison to N3, a peptidomimetic control inhibitor, high stability was observed as supported by the calculated binding energy of the M^{pro}-**P3** complex (-59.48 ± 4.87 kcal/mol). Strong interactions between **P3** and the M^{pro} active site, including four major hydrogen bonds to HIS41, ASN142, GLU166, GLN189 residues, and many hydrophobic interactions from which the interaction with CYS145 as a catalytic residue is worth mentioning. Conclusively, milk-derived bioactive peptides, especially the top five selected peptides **P1**, **P3**, **P17**, **P18**, and **P20**, show promise as an antiviral lead compound.

Keywords SARS-CoV-2 · Coronavirus · Main protease · COVID-19 · Food · Tripeptide

Introduction

Positive-strand RNA viruses include numerous pathogens and account for one-third of all virus genera (Ahlquist et al. 2003). The RNA of these viruses is translated into one or more polyproteins, which will then be cleaved by viral proteases into functional proteins. Some positive-strand RNA viruses, namely viruses from the *Coronaviridae*, *Caliciviridae*, and *Picornaviridae* families, are further classified into the picornavirus-like supercluster (Kim et al. 2012). Many classic and emerging human pathogens such as poliovirus, human rhinovirus, hepatitis A virus, as well as severe acute respiratory syndrome coronaviruses (SARS-CoV and SARS-CoV-2) are members of this supercluster. Viruses of this supercluster mainly achieve cleavage of polyproteins into mature proteins through viral 3C protease (3C^{pro}) or 3C-like protease (3CL^{pro}) (Anderson et al. 2009).

Yasaman Behzadipour and Maryam Gholampour have contributed equally to this work.

✉ Shiva Hemmati
hemmatish@sums.ac.ir

- ¹ Biotechnology Research Center, Shiraz University of Medical Sciences, PO. Box: 71345-1583, Shiraz, Iran
- ² Pharmaceutical Sciences Research Center, Shiraz University of Medical Sciences, Shiraz, Iran
- ³ Medicinal and Natural Products Chemistry Research Center, Shiraz University of Medical Sciences, Shiraz, Iran
- ⁴ Department of Medicinal Chemistry, School of Pharmacy, Shiraz University of Medical Sciences, Shiraz, Iran
- ⁵ Department of Pharmaceutical Biotechnology, School of Pharmacy, Shiraz University of Medical Sciences, Shiraz, Iran

SARS-CoV-2 from the Coronaviridae family is responsible for the COVID-19 pandemic (Moreno-Eutimio et al. 2020). The 3-chymotrypsin-like viral protease (3CL^{pro}) is the main protease of SARS-CoV-2 in charge of cleaving the polyproteins into individual functional components (Hilgenfeld 2014). The 3CL^{pro} operates on at least eleven cleavage sites on the larger polyprotein resulting in non-structural proteins 4–16 (Hemmati et al. 2020). These non-structural proteins will later assemble into a replication transcription complex crucial to viral replication (Yang et al. 2003). The 3CL^{pro}, also known as the main protease (M^{pro}), is a promising target for discovering anti-SARS-CoV-2 agents (Pillaiyar et al. 2020). SARS-CoV-2 has been mutating fast. In 2021 several variants of SARS-CoV-2 have emerged, threatening the efficacy of available vaccines and therapies (Gupta 2021; Planas et al. 2021). All of the major variants of SARS-CoV-2, namely B.1.1.7 (Alpha), B.1.351 (Beta), P.1 (Gamma), and B.1.617.2 (Delta), display mutations in their receptor-binding domain of the spike protein. Some of these mutations are N501Y (in Alpha, Beta, and Gamma variants), K417N (in Beta, and Gamma variants), E484K (in Beta, Gamma, and Delta variants), and L452R (in Delta variant) (Khateeb et al. 2021). In none of the key variants of SARS-CoV-2, a mutation in the M^{pro} has been detected (Jukič et al. 2021). This makes M^{pro} inhibitors antiviral agents with the possibility of trans-variant efficacy. Inhibitors that can block the cleavage function of M^{pro} are expected to inhibit viral replication. Because no human protease with similar cleavage specificity is known, in vivo delivery of such inhibitors faces fewer hurdles with lower side effects. Furthermore, due to the conserved regions of 3C^{pro} and 3CL^{pro} (Kim et al. 2012), inhibitors of 3CL^{pro} can be potentially utilized as broad-spectrum antivirals.

Rigorous studies have been conducted on various molecules as SARS-CoV-2 M^{pro} inhibitors (Bharadwaj et al. 2020; Gentile et al. 2020; Gurung et al. 2020). This study turns our attention to bioactive peptides of food origin with potential M^{pro} inhibitory activity. Milk proteins as a source of bioactive peptides with multifunctional properties are categorized into casein and whey proteins. Caseins are further classified into α , β , and κ caseins. Major whey proteins, on the other hand, are β -lactoglobulin and α -lactalbumin (Mohanty et al. 2016). Milk protein-derived biologically active peptides can regulate the body's physiological functions with antidiabetic, antihypertensive, antimicrobial, and anticancer effects (Sharma et al. 2021). Milk-derived bioactive peptides have been produced industrially, and a few supplemented food products are available on the market (Korhonen 2009). Among the milk-derived bioactive peptides, di- and tri-peptides (DTPs) are notably appealing for drug discovery and development because of their higher oral bioavailability, lower molecular weight, and simplicity in performing structural and quantitative structure–activity

studies. Furthermore, if necessary, the synthesis of DTPs is more cost-effective and can be easily transformed into derivatives with improved pharmacological properties (Santos et al. 2012). Various tri-peptide based molecules with protease inhibitory effects against several viruses, including dengue virus, West Nile virus (Schüller et al. 2011), human immunodeficiency virus (Mimoto et al. 2000), and hepatitis C virus (Randolph et al. 2008), have been reported. In the current study, the M^{pro} inhibitory activity of DTPs resulted from virtual proteolysis of bovine milk major proteins has been investigated. Therefore, in silico molecular docking/dynamics and interaction studies, verify if the selected milk-derived bioactive peptides can be potentially developed as anti-COVID-19 pharmaceuticals.

Materials and Methods

Virtual Digestion of Major Bovine Milk Proteins

The amino acid sequences of bovine milk major proteins were extracted from the UniProt database as follows: α S1-casein (UniProt ID: B5B3R8), α S2-casein (UniProt ID: P02663), β -casein (UniProt ID: P02666), κ -casein (UniProt ID: P02668), α -lactalbumin (UniProt ID: P00711), and β -lactoglobulin B (UniProt ID: P02754). The retrieved protein sequences were then submitted to the PeptideDB web application (<http://www4g.biotech.or.th/PeptideDB/>) to predict all the possible DTP fragments released from bovine milk major proteins (Panyayai et al. 2019). Sequences were virtually digested using all the proteases available on the PeptideDB.

Collection of Ligand and Receptor Molecules

Ligand Preparation

Three dimensional (3D) structures of peptides were energetically minimized under the Molecular Mechanics force field MM+ and then semi-empirical AM1 method using HyperChem 8.0 software (Hypercube, Canada). The Gasteiger charges (empirical atomic partial charges) and torsional degrees of freedom were assigned on the generated PDB files using AutoDockTools version 1.5.6 (Scripps Research, USA).

Preparation of M^{pro} as the Receptor

The crystal structure of SARS-CoV-2 M^{pro} in complex with a peptidomimetic molecule known as the Michael acceptor inhibitor N3 (PDB ID: 6LU7; resolution: 2.16 Å) (Jin et al. 2020) was downloaded from the protein data bank (<http://www.rcsb.org>). The preparation of protein was conducted on

AutoDockTools 1.5.6. Water molecules and the native ligand (N3) were removed from the receptor. All hydrogen atoms were added to the 6LU7 PDB, and the non-polar hydrogens were merged into the related M^{Pto} carbon atoms. Kollman charges were also assigned.

Molecular Docking Procedure

A molecular docking study between DTP as ligands and SARS-CoV-2 M^{Pto} was performed using AutoDock Vina program 1.1.2 to figure out the interacting residues. A grid box with a size of 30 × 30 × 30 Å was determined, and the cubic box was centered on the binding site of the co-crystallized ligand. The center coordinates of the grid box were attained at X: −11.6 Å, Y: 14.5 Å, and Z: 68.3 Å and the exhaustiveness was set to be 100. Other docking parameters were set as default. The results were visualized with the Discovery Studio Client 2017 software.

Absorption, Distribution, Metabolism, Excretion, and Toxicity (ADMET) Analyses

The Drug-likeness of the peptides was evaluated on the SwisADME online server (<http://www.swissadme.ch/>) using the Lipinski filter (Lipinski 2000). ADMET properties and some physicochemical parameters were predicted using the admetSAR online tool (<http://lmmd.ecust.edu.cn/admetSar1/predict/>) (Yang et al. 2019). Allergenicity and hemolytic activity of peptides were predicted employing AllergenFP (Dimitrov et al. 2013) and HemoPI servers (Chaudhary et al. 2016). The HemoPI server also provided the isoelectric points of peptides.

Molecular Dynamics Simulation Study

The molecular dynamics simulation (MD) technique was performed as previously described by Pirhadi et al. (Pirhadi et al. 2020). Briefly, the MD study was carried out for the complex of the M^{Pto} with P3 as an inhibitor and the N3 ligand (Jin et al. 2020) as a peptidomimetic control, using the Gromacs 2019 simulation package for the period of 100 ns on a GPU server. Amber99sb force field at a mean temperature of 300 K and the physiological pH of 7.0 was applied. Chimera software was implemented to calculate AM1 partial charges. Using the acpype program, the topology and coordinate files of P3 as a milk-derived inhibitor and N3 were created. After adding water molecules to the protein complex model, the system was neutralized by adding Na⁺/Cl[−] ions. The equilibration of the system (NVT and NPT ensembles) was performed in two steps for 500 ps. The atom positions of M^{Pto} complexes were restrained by force constant of 1000 kJ mol^{−1} nm^{−2}. The production MD was then run for 100 ns time. A pressure of one bar and a

temperature of 300 K were kept constant during the simulation to achieve a stable state. To regulate the temperature inside the box V-rescale thermostat was used. The PME (particle-mesh Ewald) method was employed to designate the long-range electrostatic interactions. Furthermore, the LINCS algorithm constrained the length of covalent bonds. Finally, after completing of the MD simulation, we calculated the root-mean-square deviation (RMSD) to identify the equilibrium time range to calculate root-mean-square fluctuation (RMSF) and the total number of hydrogen-bonding interactions. Finally, the binding free energies between the components of complexes was calculated using the MM-PBSA (MM-Poisson–Boltzmann surface area) method during the last 10 ns of the trajectory files (Kumari et al. 2014).

Results and Discussion

Identification of Bovine Milk-Derived DTPs

Currently, peptides have become increasingly appealing as biotherapeutics. Although peptides occupy a small portion of the global drug market for the time being, their future is boundless due to their high selectivity, high binding affinity, and limited risk of drug-drug interactions and side effects (Di 2015). Also, bioactive peptides encrypted in the native protein sequences with their natural compositions and health-promoting effects can be considered promising compounds for developing nutraceutical or functional foods.

On account of their antiviral activity reports among many health-enhancing properties (Pan et al. 2006), milk-derived peptides were selected for further study as potential anti-SARS-CoV-2 agents. Major proteins of bovine milk were digested using 34 different proteases and chemicals available in FEPTideDB, including digestive enzymes such as high and low specificity chymotrypsin, pepsin (pH 1.3 and 2.0), and trypsin, as well as non-digestive enzymes such as clostripain, caspases, and thrombin. FeptideDB is used to forecast the bioactive peptides from food proteins. Digestions resulted in 142 unique dipeptides and 184 unique tripeptides. DTPs resulted from the digestion of bovine milk major proteins are available in supplementary material 1.

Molecular Docking Study

SARS-CoV-2 M^{Pto} is a dimer. Each monomer is made up of three domains as follows: domain I (residues 8–101), domain II (residues 102–184), and domain III (residues 201–303). Domains I and II mainly form β-sheets, and domain III is α-helical. While domain II and domain III are connected by a loop (residues 185–200), the substrate-binding site can be found between domains I and II (Fig. 1) (Zhang et al. 2020). Contrary to other cysteine proteases with a catalytic triad in

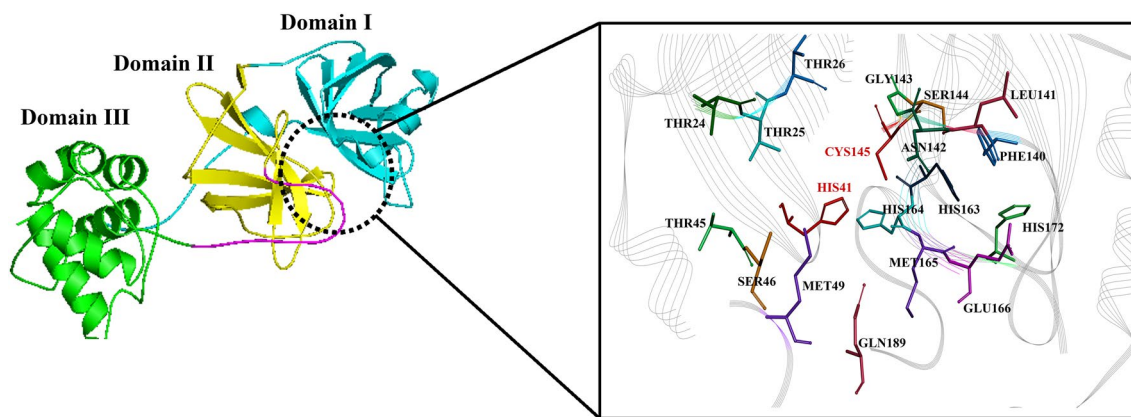


Fig. 1 A schematic representation of SARS-CoV-2 M^{PRO}, depicting three domains of the enzyme (Domain I, Domain II, and Domain III), the position of enzyme active site, and the placement of residues in the enzyme's active site, including the catalytic dyad HIS41 and CYS145

the active site of M^{PRO}, CYS145 and HIS41 form a catalytic dyad without any third residue (Anand et al. 2003).

Molecular docking was performed for a total of 326 DTPs. The energy of binding for all 326 peptides is available in supplementary material 1. It could be observed that, on average, milk-derived tripeptides had a stronger binding affinity to M^{PRO} compared with dipeptides. Out of all the analyzed peptides, twenty peptides with the best binding energies ($\Delta G_b < -7$ kcal/mol) were selected. The top 20 peptides named **P1–P20** are shown in Table 1, including their sequence, binding energy, inhibition constant (K_i), and hydrogen bonding interactions with amino acid residues in the enzyme active site. It can be perceived from Table 1 that 80% of the 20 selected peptides have an aromatic-hydrophobic amino acid residue (phenylalanine/tyrosine/tryptophan) at their C-terminal. In contrast, peptides with GLN as their first or second residue formed a higher number of interactions. It should be noted that in the M^{PRO}, the cleavage recognition site mostly consists of “Leu-Gln↓(Ser, Ala, Gly)” (↓ showing the cleavage position) (Zhang et al. 2020). A fingerprint of all the hydrogen bonding interactions between the top 20 peptides and amino acid residues of the M^{PRO} is provided in Fig. 2.

As shown in Fig. 2, milk-derived DTPs could form the highest number of interactions with the catalytic residue CYS145. Moreover, **P1** is the ligand with the highest binding affinity, and **P17** can be recognized as the ligand with the highest number of interactions. The ligands were stabilized by forming several strong interactions with M^{PRO} residues, among which hydrogen bonding interactions warrant special consideration. Peptides **P1**, **P3**, **P17**, **P18**, and **P20** could form a high number of hydrogen bonding interactions with amino acids present in the active site of M^{PRO} with high binding affinity. It should be noted that all five peptides formed at least two hydrogen bonds with the catalytic residue CYS145. Meanwhile, **P1** and **P17** were able to form a

π -alkyl hydrophobic interaction with the other catalytic residue HIS41. The interactions of selected five peptides with the M^{PRO} of SARS-CoV-2 are portrayed in Fig. 3. These five peptides are selected as the most promising peptides against M^{PRO} for further analyses of all milk-derived DTPs.

P3, **P18**, and **P20** are derived from the proteolysis of β -casein, β -lactoglobulin, and α -S2-casein using proteinase K, respectively. **P1** can be obtained through digesting β -lactoglobulin using chymotrypsin, and **P17** is originated from the lysis of α -S1-casein by pepsin (pH 1.3). Digestion of β -casein with pepsin (pH 1.3), chymotrypsin, and trypsin can also result in **P3**. Therefore, among five selected peptides, **P1**, **P3** and **P17** can be released from the gastrointestinal digestion of bovine milk. However, to verify if the gastrointestinal digestion of bovine milk can result in adequate therapeutic concentrations of **P1**, **P3**, and **P17** against SARS-CoV-2 needs further in vivo trials.

It is of note that there is evidence of gastrointestinal absorption of some DTPs in our study. Antihypertensive peptides **FY** (ΔG_b : -6.8 kcal/mol), **LY** (ΔG_b : -6.5 kcal/mol), **VPP** (ΔG_b : -5.4 kcal/mol), **IPP** (ΔG_b : -5.3 kcal/mol), and **VY** (ΔG_b : -5.3 kcal/mol) are among the peptides that could be detected in the bloodstream after oral administration (Xu et al. 2019b).

ADMET and Physicochemical Properties of the Five Selected Peptides

While in vivo pharmacokinetic studies are the most conclusive for the investigation of absorption, distribution, metabolism, excretion, and toxicity (ADMET) properties of therapeutics, in silico studies of such properties would assist scientists to save valuable resources in the early stages of drug discovery.

DTPs are at the boundary between peptides and small molecules and can be treated as either in certain situations.

Table 1 Results of docking study for the top 20 peptides with the best binding energies

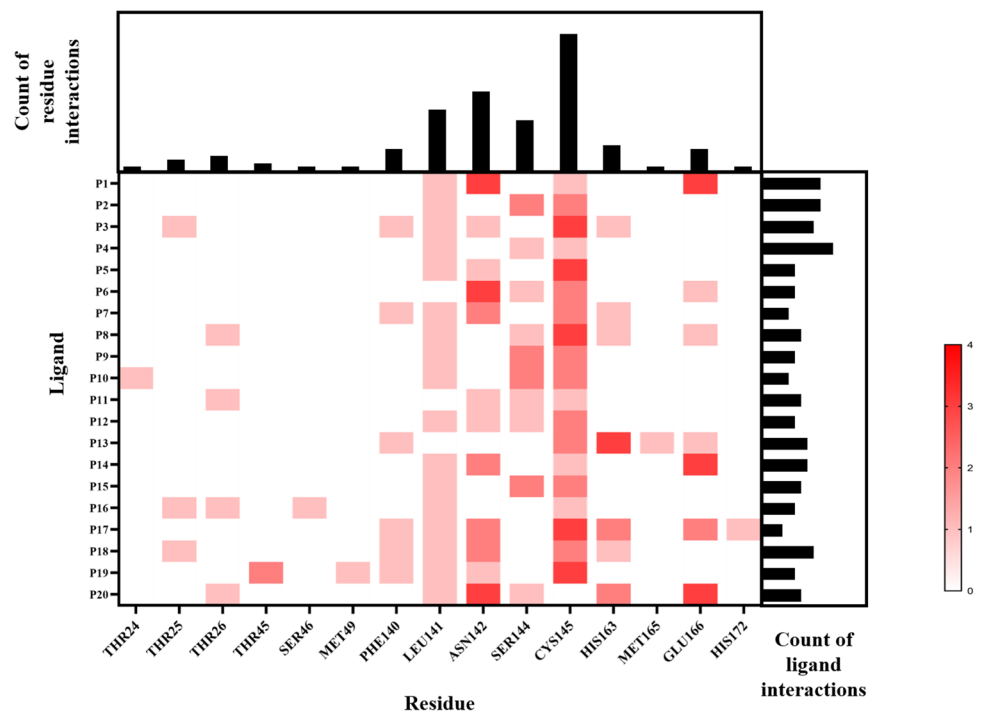
Ligand name	Ligand sequence	ΔG_b (kcal/mol)	K_i (μ M)	Hydrogen bonds between ligand and receptor	Distance (\AA)	Ligand name	Ligand sequence	ΔG_b (kcal/mol)	K_i (μ M)	Hydrogen bonds between ligand and receptor	Distance (\AA)
P1	RVY	- 7.7	2.2	LEU141	2.80	P11	QKW	- 7.2	5.2	THR26	2.85
				ASN142	3.53					ASN142	3.45
				ASN142	3.19					SER144	2.94
				GLU166	3.30					CYS145	3.26
P2	PEW	- 7.5	3.1	ASN142	3.13	P12	NQF	- 7.1	6.2	CYS145	4.21
				CYS145	3.05					CYS145	3.59
				CYS145	3.75					LEU141	2.82
				CYS145	3.71					SER144	3.06
				CYS145	4.18					ASN142	2.86
				CYS145	2.93					CYS145	3.29
P3	QSW	- 7.5	3.1	LEU141	3.24	P13	FH	- 7.1	6.2	GLU166	3.05
				SER144	2.89					CYS145	3.13
				SER144	2.89					CYS145	3.51
				CYS145	4.02					PHE140	3.32
				CYS145	4.30					HIS163	2.85
				ASN142	3.58						
				THR25	3.20						
P4	PLW	- 7.4	3.7	LEU141	3.15	P14	RF	- 7.1	6.2	LEU141	3.12
				PHE140	3.02					ASN142	3.05
				CYS145	3.11					CYS145	3.09
				HIS163	3.06					ASN142	3.45
				LEU141	2.84					CYS145	3.81
P5	LLY	- 7.4	3.7	SER144	2.89	P15	PSF	- 7.0	7.3	CYS145	4.14
				CYS145	4.25					CYS145	4.14
				ASN142	3.28					LEU141	2.93
				LEU141	2.85					SER144	3.26
				CYS145	3.10					SER144	2.9
				CYS145	4.20					CYS145	3.49
P6	RQF	- 7.3	4.4	SER144	3.04	P16	LGY	- 7.0	7.3	SER145	2.94
				ASN142	3.48					SER46	3.52
				ASN142	3.09					THR25	2.95
				ASN142	3.07					THR26	3.21
				CYS145	4.12					LEU141	
				CYS145	3.66						

Table 1 (continued)

Ligand name	Ligand sequence	ΔG_b (kcal/mol)	K_i (μ M)	Hydrogen bonds between ligand and receptor	Ligand name	Ligand sequence	ΔG_b (kcal/mol)	K_i (μ M)	Hydrogen bonds between ligand and receptor	Residues of receptor		Distance (\AA)
										Residues of receptor	Distance (\AA)	
P7	QW	- 7.3	4.4	LEU141	P17	DAY	- 7.0	7.3	CYS145	Residues of receptor	Distance (\AA)	3.13
				ASN142					CYS145			3.89
				CYS145					ASN142			4.21
				PHE140					LEU141			3.26
				CYS145					ASN142			3.14
P8	DQW	- 7.2	5.2	HIS163	P18	QSA	- 7.0	7.3	CYS145	Residues of receptor	Distance (\AA)	3.05
				ASN142					CYS145			3.06
				CYS145					GLU166			3.34
				PHE140					PHE140			3.58
				HIS163					HIS163			3.03
P9	PQY	- 7.2	5.2	GLU166	P19	QSE	- 7.0	7.3	GLU166	Residues of receptor	Distance (\AA)	3.58
				CYS145					HIS172			3.69
				GLU166					LEU141			3.13
				CYS145					ASN142			3.03
				THR26					PHE140			3.00
P10	PSY	- 7.2	5.2	LEU141	P20	RNA	- 7.0	7.3	CYS145	Residues of receptor	Distance (\AA)	3.99
				SER144					CYS145			2.99
				CYS145					HIS163			3.20
				GLU166					ASN142			3.71
				SER144					THR25			3.57
P11	QW	- 7.3	4.4	LEU141	P17	DAY	- 7.0	7.3	CYS145	Residues of receptor	Distance (\AA)	3.89
				ASN142					CYS145			4.21
				CYS145					ASN142			3.26
				PHE140					LEU141			3.14
				CYS145					ASN142			3.05
P12	DQW	- 7.2	5.2	HIS163	P18	QSA	- 7.0	7.3	CYS145	Residues of receptor	Distance (\AA)	3.06
				ASN142					CYS145			3.06
				CYS145					GLU166			3.34
				PHE140					PHE140			3.58
				HIS163					HIS163			3.03
P13	PQY	- 7.2	5.2	GLU166	P19	QSE	- 7.0	7.3	GLU166	Residues of receptor	Distance (\AA)	3.58
				CYS145					HIS172			3.69
				GLU166					LEU141			3.13
				CYS145					ASN142			3.03
				THR26					PHE140			3.00
P14	PSY	- 7.2	5.2	LEU141	P20	RNA	- 7.0	7.3	CYS145	Residues of receptor	Distance (\AA)	3.99
				SER144					CYS145			2.99
				CYS145					HIS163			3.20
				GLU166					ASN142			3.71
				SER144					THR25			3.57

 ΔG_b binding free energy, K_i inhibition constant

Fig. 2 Hydrogen bonding fingerprint for the top 20 milk-derived peptides (**P1–P20**) with SARS-CoV-2 M^{pro}. Different shades show the number of interactions between a peptide and an enzyme residue (the darkest shade accounts for four interactions between the ligand and a specific residue). The total count of residue interactions and the total count of ligand interactions are also represented



Because of low molecular weight, they can be analyzed for drug-likeness based on Lipinski's rule of five. Lipinski's rule of five is used to determine whether a compound is likely to be orally active in humans. It should be mentioned that the bioavailability of DTPs is also regulated by factors beyond those influencing the small molecules. One of the main factors that set apart the ADMET properties of DTPs from those of small molecules and larger peptides is their cellular uptake by peptide transporters (PEPTs) called PEPT1 and PEPT2. Peptide transporters are a group of integral cellular membrane proteins. These transporters can be primarily found in the epithelial cells of the bile duct, kidneys, lungs, and small intestine, where they mediate the cellular uptake of DTPs. These transporters can transport most naturally occurring DTPs inside cells regardless of their sequence (Prudhomme 2013). This potential lung tropism of DTPs is beneficial, given that COVID-19 affects the lungs. PEPTs are also involved in the oral absorption of DTPs (Xu et al. 2019a). These transporters in kidneys mediate reabsorption of DTPs from the glomerular filtrate, therefore, increasing the potential plasma half-life of DTPs (Rubio-Aliaga and Daniel 2008).

As part of the ADMET properties investigation, drug-likeness and plasma-protein binding of five selected peptides (**P1**, **P3**, **P17**, **P18**, **P20**) were determined (Table 2). Based on the ADMET properties, only the characteristics of **P1** and **P20** were not in line with Lipinski's rule of five. Furthermore, **P1**, **P3**, and **P17** were predicted to have more than 30% human intestinal absorption. None of the five selected peptides showed a high degree of plasma protein

binding. Therefore, they can readily diffuse through tissues after administration (Leach et al. 2006). The clinical manifestations of SARS-CoV-2 have expanded to include neurological symptoms as well, and the virus itself has been detected in CNS tissue (Paniz-Mondolfi et al. 2020). Therefore, it is essential that the proposed therapeutic agents pass the blood–brain barrier (BBB) and penetrate the CNS tissue. Except for **P1** and **P17**, the other three peptides were predicted to be BBB positive. Cytochrome P450 inhibition by a therapeutic can potentially lead to clinical drug–drug interactions (Cheng et al. 2011). Based on our analyses, none of the five selected peptides was significant inhibitors of cytochrome P450 (Table 2).

Some physicochemical properties are determinative to the peptide further development as therapeutics. Among them, solubility and isoelectric point (pI) are noteworthy (Behzadipour and Hemmati 2019). Experimental procedures and formulation of therapeutics usually require highly concentrated samples; therefore, the low water solubility of peptides is unfavorable. Isoelectric point values are important since they can affect the solubility of a molecule at a certain pH. Usually, the solubility of a peptide decreases at a pH near that of its pI. For an optimal solubility profile, the pI of the peptide should not be close to the physiologic pH. Peptides **P1**, **P17**, and **P20** had higher water solubility (Table 2). None of the peptides had a pI near 7.4.

Hemolysis, allergenicity, and carcinogenicity are among the possible side effects of peptides and peptide-based therapeutics (Shankar et al. 2014; Win et al. 2017). Among the five selected peptides, none of them was predicted as

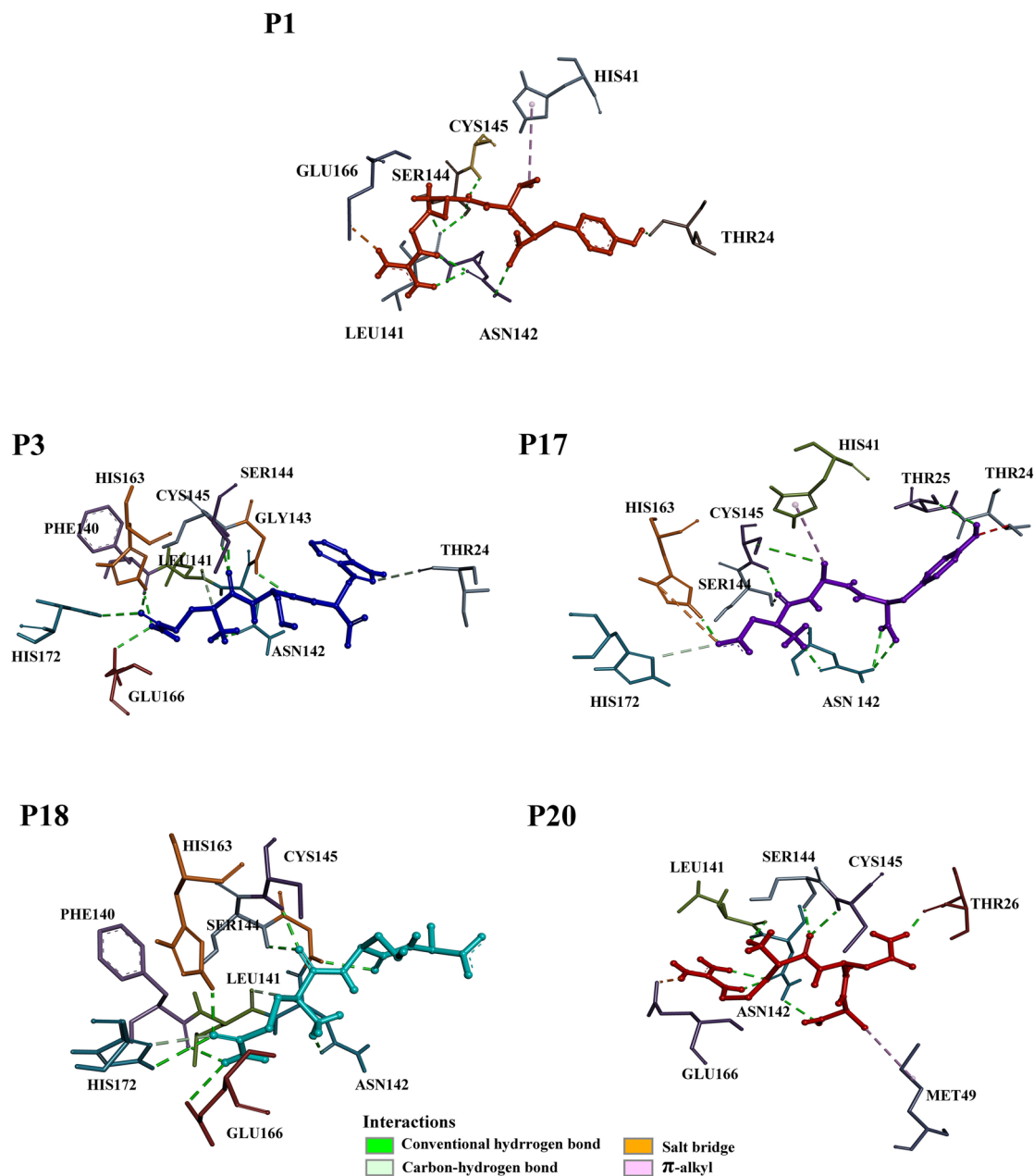


Fig. 3 Different interactions between five selected peptides (**P1**, **P3**, **P17**, **P18**, **P20**) and amino acid residues in the active site of SARS-CoV-2 M^{Pro} (The green dash line represents a conventional hydrogen

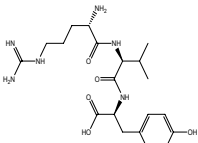
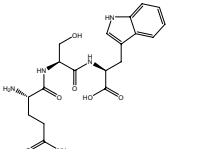
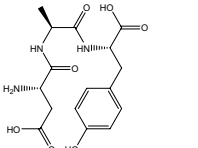
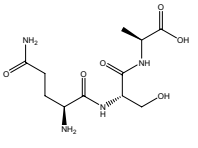
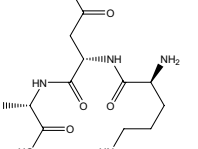
bond; the orange dash line is a salt bridge; the light green dash line displays a carbon-hydrogen bond, and the pink dash line designates a π -alkyl bond) (Color figure online)

hemolytic or carcinogenic; however, **P1**, **P17** and **P18** were predicted as probable allergens (Table 3). None of the five selected peptides is expected to cause acute oral toxicity in the case of oral administration ($LD_{50} > 500 \text{ mg} \cdot \text{kg}^{-1}$). Altogether, peptide **P3** had the most favorable ADMET properties. Therefore, among the most promising milk-derived DTP, **P3** was selected for MD simulation analysis.

Molecular Dynamics Simulation Study

MD simulation is applied to the ligand-receptor complex to shed light on the stability and interactions in the matter of time (Rahmatabadi et al. 2019). An MD simulation analysis of 100 ns was performed for the SARS-CoV-2 M^{Pro} in complex with **P3** and **N3** as further validation of

Table 2 ADME and physicochemical properties of the five selected milk-derived peptides as SARS-CoV-2 M^{PTO} inhibitors

Ligand name	Ligand structure	Physicochemical properties			ADME properties				
		Mw (Da)	Water solubility (logS)	pI	Drug-likeness	Human intestinal absorption	Blood–brain barrier penetration	Plasma-protein binding (%)	Cytochrome P450 inhibition
P1		436	− 3.1	9.1	✗	✓	✗	0.7	✗
P3		420	− 1.9	5.9	✓	✓	✓	0.5	✗
P17		367	− 2.6	3.8	✓	✓	✗	0.7	✗
P18		304	− 0.7	5.9	✓	✗	✓	0.1	✗
P20		359	− 2.0	10.1	✗	✗	✓	0.3	✗

Drug-likeness: follows Lipinski's rule of five, does not follow Lipinski's rule of five; Human intestinal absorption: higher than 30% intestinal absorption, lower than 30% intestinal absorption; Blood–brain barrier: passes blood–brain barrier, does not pass blood–brain barrier; Cytochrome P inhibition y: high P450 promiscuous inhibitory compound, low P450 promiscuous inhibitory compounds

Table 3 Toxicity evaluation of the five selected milk-derived peptides as SARS-CoV-2 M^{PTO} inhibitors

Ligand name	Hemolytic potential	Allergenicity	Carcinogenicity	Oral toxicity
P1	✗	✓	✗	✗
P3	✗	✗	✗	✗
P17	✗	✗	✗	✗
P18	✗	✓	✗	✗
P20	✗	✗	✗	✗

Hemolytic potential: Hemolytic:✓, non-hemolytic:✗; Allergenicity: allergen:✓, non-allergen:✗; Carcinogenicity: carcinogen:✓, non-carcinogen:✗; Oral toxicity: oral LD50 < 500 mg kg⁻¹:✓, oral LD50 > 500 mg kg⁻¹:✗

our previous results and to evaluate the binding mode and the stability of interactions of **P3** against the enzyme. RMSD analysis was used to assess the convergence of simulation. Figure 4 shows the backbone RMSD values of the M^{PTO}-**P3** complex as a function of time (ns) over the entire simulation. After the selected equilibrium time for the M^{PTO}-**P3** complex (15 ns), the complex shows excellent stability until simulation's end. Low RMSD values and fluctuations during simulation (0.18 ± 0.12 nm) indicate a stable complex formation. In comparison, the M^{PTO}-**N3** complex reaches equilibrium at 75 ns. The MD trajectory after 15 ns for **P3** and after 75 ns for **N3** was considered for any further analyses. Moreover, the RMSF values of the backbone atoms for all residues for both complexes

were calculated. No RMSF values greater than 2 nm were observed (Fig. 5).

The hydrogen bond interactions were monitored between the ligands and amino acid residues of the enzyme active site during the equilibrium time range. Four major hydrogen bonds to His41, ASN142, GLU166, and GLN189 residues with a lifetime of above 10% were observed for both

ligands during their respective equilibrium time frames. **P3**'s hydrogen bonds with GLU166 and GLN189 showed higher stability between these four hydrogen bonds, while hydrogen bonds with ASN142 and HIS41 had lower stability. Hydrogen bonds that **N3** formed with HIS41 and GLN189 were more stable. The hydrogen bonds with ASN142 and GLU166 for **N3** were not as stable as the other two hydrogen

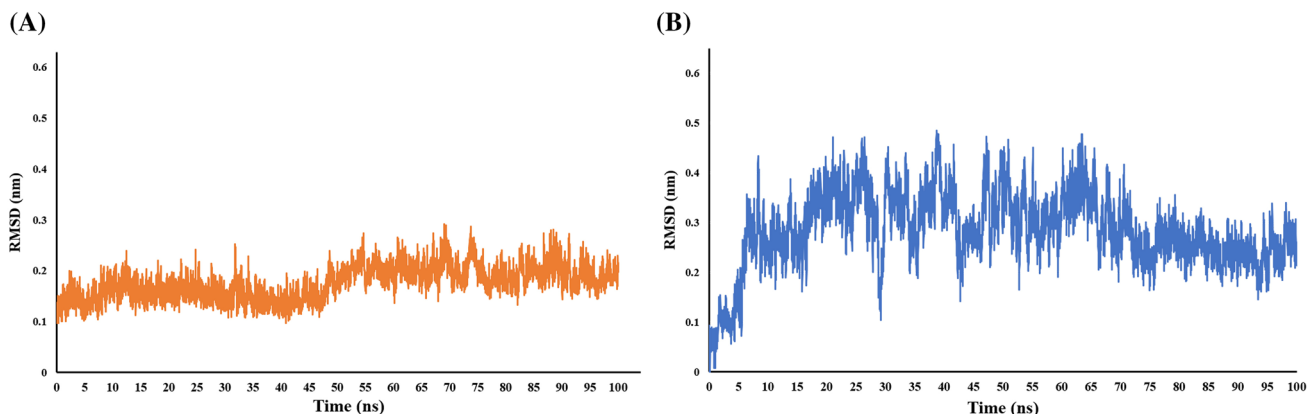


Fig. 4 The RMSD values (nm) for the backbone atoms of **A P3-M^{PTO}** complex and **B N3-M^{PTO}** complex plotted versus time (ns)

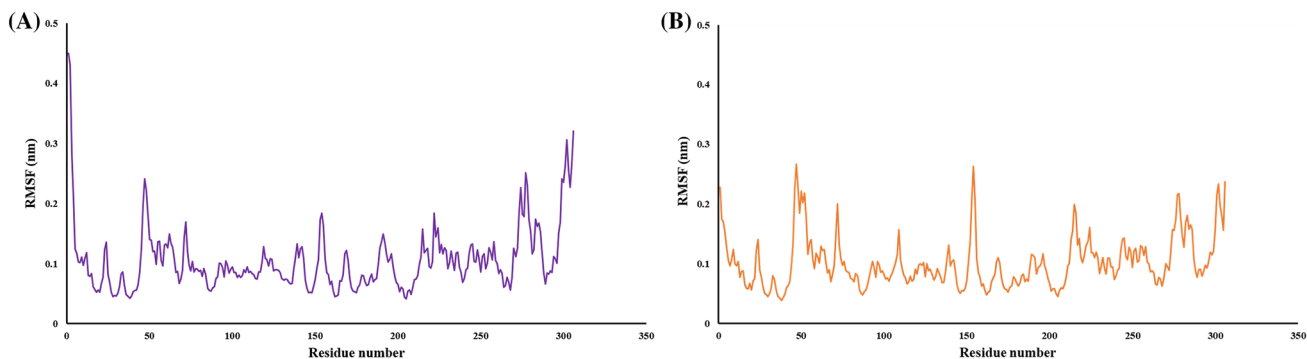


Fig. 5 The RMSF values (nm) of SARS-CoV-2 **M^{PTO}** residues in complex with **A P3** and **B N3**

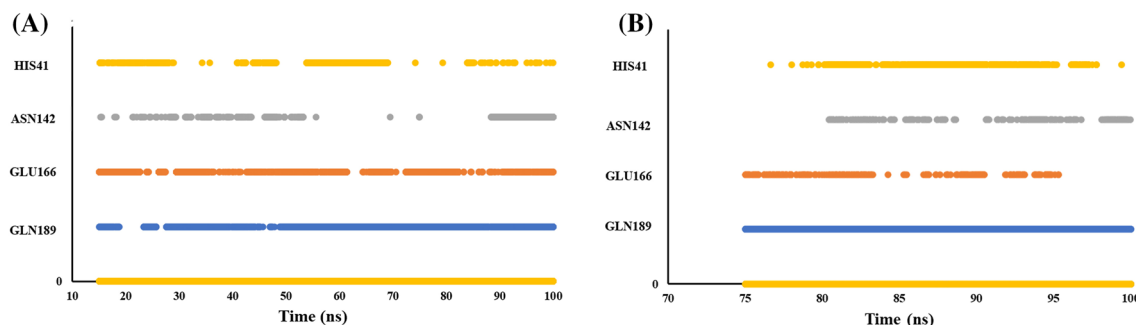


Fig. 6 The occurrence of hydrogen bonds as a function of time between **A P3** and amino acid residues HIS41 (lifetime: 11.78%), ASN142 (lifetime: 10.90), GLU166 (lifetime: 31.52%), GLN189

(lifetime: 51.89%) as well as **B N3** and HIS41 (lifetime: 38.74%), ASN142 (lifetime: 16.16%), GLU166 (lifetime: 12.6%), GLN189 (lifetime: 98.00%) of SARS-CoV-2 **M^{PTO}**

bonds. The occurrence of hydrogen bonds as a function of time between the ligands and enzyme residues is shown in Fig. 6. Two of the four major hydrogen bonds can be observed in the docking of **P3** as well. Other hydrogen bonds from docking (CYS145, ASN142, THR25, LEU141, PHE140, HIS163) were transient in the simulation study (lifetime less than 10%).

The cluster analysis of the M^{pro} -**P3** and M^{pro} -**N3** complexes using the Gromos method and a cut-off value of 0.2 created three clusters for each complex. The first representative frames accounted for more than 90% of total snapshots. Therefore, the representative frames of cluster 1, as the most representative frame of the simulation, were chosen for the interaction analysis of **P3** and **N3**. As can be seen from the interactions of cluster 1 of M^{pro} -**P3** complex (Fig. 7), hydrogen bonding interactions were formed between the amine group of GLN residue of **P3** and GLN189, and the carboxyl group of TRP residue of **P3** with MET165 and GLU166 in the active site of M^{pro} . However, the hydrogen bonding interaction of MET165 was not stable during the equilibrium time range of the simulation. Various hydrophobic interactions between **P3** and the catalytic residue of CYS145 and the other critical residues of the M^{pro} , such as LEU141 and, HIS164 can be observed in Fig. 7.

The 3D structure of the docked **P3** orientation in the M^{pro} active site compared to its cluster representative from the simulation study is available in Fig. 8. As it is clear from the figure, **P3** has moved in the enzyme active site compared to its initial input structure, and this movement resulted in a

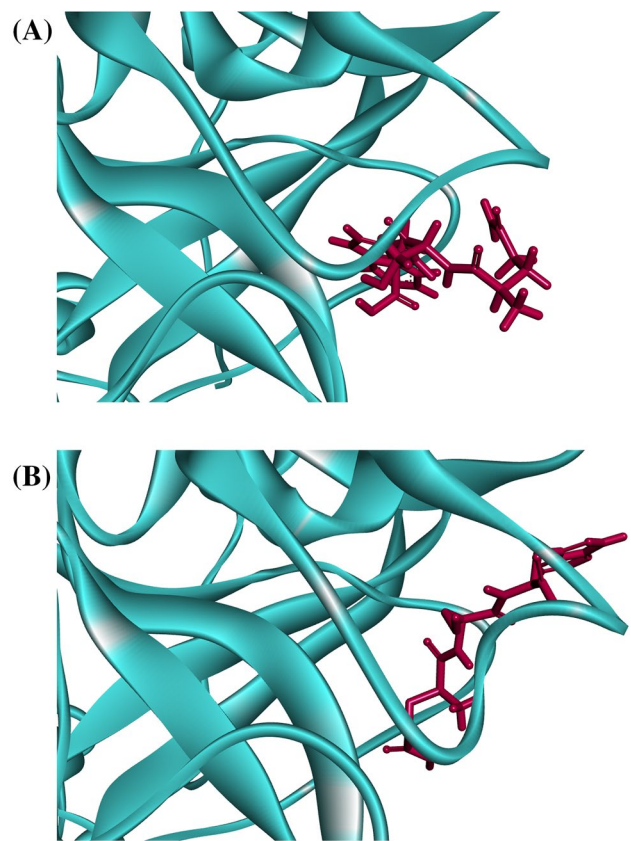


Fig. 8 The comparison of the **P3** molecule orientation in the M^{pro} active site between the docking and the MD simulation studies **A** orientation of **P3** molecule in the cluster 1 representative of MD simulation study and **B** orientation of **P3** molecule in the docking study

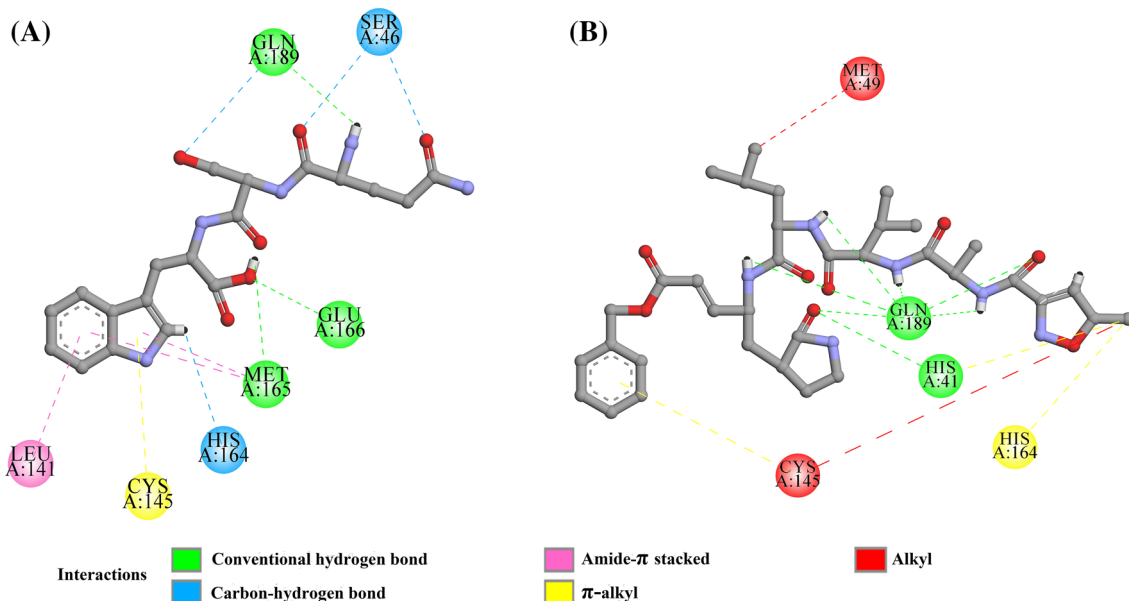


Fig. 7 2D profile of different interactions formed between **A** **P3**, **B** **N3** and amino acid residues in the active pocket of SARS-CoV-2 M^{pro} in cluster 1 representative of MD simulation (The green dash line rep-

resents a conventional hydrogen bond; the pink dash line designates an amide- π stacked; the blue dash line displays a carbon-hydrogen bond, and the yellow dash line is a π -alkyl bond) (Color figure online)

Table 4 Binding free energy components (Kcal/mol) of P3 and N3 in complex with M^{pro}

Complex	Van der Waals energy	Electrostatic energy	Polar solvation energy	SASA energy	Binding energy
M ^{pro} -N3	- 55.22 ± 4.15	- 5.63 ± 1.50	31.53 ± 3.18	- 5.75 ± 0.32	- 35.07 ± 4.28
M ^{pro} -P3	- 40.72 ± 2.68	- 73.48 ± 10.66	58.99 ± 14.19	- 4.27 ± 0.20	- 59.48 ± 4.87

different binding interaction pattern. Some of the residues involved in initial hydrogen bonding with **P3** have formed hydrophobic interactions. Except for ASN142, new hydrogen bonding interactions have been established between **P3** and the active site of the M^{pro}. No π - π interactions were observed in three cluster representatives as well as in the docking study.

To evaluate the affinity of **P3** to M^{pro} in comparison to **N3**, the binding free energies of both ligands to M^{pro} were calculated using the Poisson-Boltzmann surface area (MM-PBSA) method (Table 4). In the last 10 ns of the simulation, **P3** showed a higher affinity to the active site of M^{pro} ($\Delta G_b = -59.48 \pm 4.87$ kcal/mol) compared to **N3** ($\Delta G_b = -35.07 \pm 4.28$ kcal/mol). The significant difference between the electrostatic energies of M^{pro}-**P3** and M^{pro}-**N3** complexes, among other components of binding free energies, reveals stronger polar interactions for the binding of **P3** to the active site of M^{pro} compared to **N3**.

Although various peptides and peptidomimetics have been tested against SARS-CoV-2 using different methods, no previous reports of evaluation of 3CL^{pro} inhibitory food-derived di- and tri-peptides have been reported. At the beginning of the COVID-19 pandemic, lopinavir and ritonavir peptide-based HIV protease inhibitors were used in clinical trials as a potential treatment (Apostolopoulos et al. 2021). Molecules, such as the α -ketoamides (Zhang et al. 2020), and peptidomimetic aldehydes (Dai et al. 2020), showed high levels of M^{pro} inhibition with an IC₅₀ of about 0.67 μ M and 0.05 μ M, respectively. Furthermore, virtual screening approaches have identified a variety of peptide-based compounds as potential M^{pro} inhibitor candidates. Evaluation of soy cheese peptides (Chourasia et al. 2020), beta-lactoglobulin-derived bioactive peptides (Çakır et al. 2021), and several milk-derived peptides with 5–13 amino acid residues (Pradeep et al. 2021) are examples of such screenings. However, it is of particular note that compared to other naturally derived bioactive compounds, di- and tri-peptides such as **P3** in the current study have several advantages, including higher bioavailability, cost-effective synthesis and chemical modification.

Conclusion

In this study, we evaluated the protease inhibitory potential of milk-derived peptides against SARS-CoV-2 M^{pro}. Several milk-derived DTPs have a favorable binding affinity and can form critical interactions with the active site of SARS-CoV-2 M^{pro}, among which **P1**, **P3**, **P17**, and **P20** were the best inhibitor candidates. According to the MD simulation results, the M^{pro}-**P3** complex as a sample showed high stability as well. Some of the studied peptides can be produced by the gastrointestinal digestion of bovine milk. Therefore, the presence of adequate bovine milk in the food regimen might be beneficial against COVID-19, yet to inhibit SARS-CoV-2 M^{pro}, these peptides should be synthesized and formulated as a dosage form. Notably, the cellular uptake of such tri-peptides is mediated by peptide transporters found in the epithelial cells of the lungs and small intestine. This potential lung tropism of DTPs is beneficial, given that COVID-19 dominantly affects the lungs. In conclusion, bioactive peptides have the potential to be used as inhibitors against SARS-CoV-2 and potentially other positive-strand RNA viruses from picornavirus-like supercluster.

Supplementary Information The online version contains supplementary material available at <https://doi.org/10.1007/s10989-021-10284-y>.

Acknowledgements The authors would like to thank Shiraz University of Medical Sciences, Shiraz, IRAN for the financial support of this work (Grant number 99-01-05-23159).

Author Contributions YB: Formal analysis, Investigation, Writing—Original Draft; MG: Formal analysis, Writing—Original Draft, Visualization; SP: Software, Data Curation; HS: Validation, Writing—Review and Editing; MK: Methodology, Validation; SH: Conceptualization, Resources, Writing—Review and Editing, Supervision, Project administration.

Funding This study was funded by Shiraz University of Medical Sciences (Grant number 99-01-05-23159).

Declarations

Conflict of interest The authors declare that there is no conflict of interest.

Ethical Approval IR.SUMS.REC.1399.569.

References

- Ahlquist P, Noueiry AO, Lee W-M, Kushner DB, Dye BT (2003) Host factors in positive-strand RNA virus genome replication. *J Virol* 77:8181–8186. <https://doi.org/10.1128/JVI.77.15.8181-8186.2003>
- Anand K, Ziebuhr J, Wadhvani P, Mesters JR, Hilgenfeld R (2003) Coronavirus main proteinase (3CLpro) structure: basis for design of anti-SARS drugs. *Science* 300:1763–1767. <https://doi.org/10.1126/science.1085658>
- Anderson J, Schiffer C, Lee S-K, Swanstrom R (2009) Viral protease inhibitors. In: Kräusslich H-G, Bartenschlager R (eds) *Antiviral strategies*. Springer Berlin Heidelberg, Berlin, Heidelberg, pp 85–110
- Apostolopoulos V, Bojarska J, Chai T-T, Elnagdy S, Kaczmarek K, Matsoukas J, New R, Parang K, Lopez OP, Parhiz H, Perera CO, Pickholz M, Remko M, Saviano M, Skwarczynski M, Tang Y, Wolf WM, Yoshiya T, Zabrocki J, Zielenkiewicz P, AlKhazindar M, Barriga V, Kelaidonis K, Sarasia EM, Toth I (2021) A global review on short peptides: frontiers and perspectives. *Molecules* 26:430
- Behzadipour Y, Hemmati S (2019) Considerations on the rational design of covalently conjugated cell-penetrating peptides (CPPs) for intracellular delivery of proteins: a guide to CPP selection using glucarpidase as the model cargo molecule. *Molecules* 24:4318. <https://doi.org/10.3390/molecules24234318>
- Bharadwaj S, Lee KE, Dwivedi VD, Kang SG (2020) Computational insights into tetracyclines as inhibitors against SARS-CoV-2 Mpro via combinatorial molecular simulation calculations. *Life Sci* 257:118080
- Çakır B, Okuyan B, Şener G, Tunali-Akbay T (2021) Investigation of beta-lactoglobulin derived bioactive peptides against SARS-CoV-2 (COVID-19): in silico analysis. *Eur J Pharmacol* 891:173781. <https://doi.org/10.1016/j.ejphar.2020.173781>
- Chaudhary K, Kumar R, Singh S, Tuknait A, Gautam A, Mathur D, Anand P, Varshney GC, Raghava GPS (2016) A web server and mobile app for computing hemolytic potency of peptides. *Sci Rep* 6:22843. <https://doi.org/10.1038/srep22843>
- Cheng F, Yu Y, Zhou Y, Shen Z, Xiao W, Liu G, Li W, Lee PW, Tang Y (2011) Insights into molecular basis of cytochrome P450 inhibitory promiscuity of compounds. *J Chem Inf Model* 51:2482–2495. <https://doi.org/10.1021/ci200317s>
- Chourasia R, Padhi S, Chiring Phukon L, Abedin MM, Singh SP, Rai AK (2020) A potential peptide from soy cheese produced using *Lactobacillus delbrueckii* WS4 for effective inhibition of SARS-CoV-2 main protease and S1 glycoprotein. *Front Mol Biosci* 7:601753. <https://doi.org/10.3389/fmolb.2020.601753>
- Dai W, Zhang B, Jiang X-M, Su H, Li J, Zhao Y, Xie X, Jin Z, Peng J, Liu F, Li C, Li Y, Bai F, Wang H, Cheng X, Cen X, Hu S, Yang X, Wang J, Liu X, Xiao G, Jiang H, Rao Z, Zhang L-K, Xu Y, Yang H, Liu H (2020) Structure-based design of antiviral drug candidates targeting the SARS-CoV-2 main protease. *Science* 368:1331. <https://doi.org/10.1126/science.abb4489>
- Di L (2015) Strategic approaches to optimizing peptide ADME properties. *AAPS J* 17:134–143. <https://doi.org/10.1208/s12248-014-9687-3>
- Dimitrov I, Naneva L, Doytchinova I, Bangov I (2013) AllergenFP: allergenicity prediction by descriptor fingerprints. *Bioinformatics* 30:846–851. <https://doi.org/10.1093/bioinformatics/btt619>
- Gentile D, Patamia V, Scala A, Sciortino MT, Piperno A, Rescifina A (2020) Putative inhibitors of SARS-CoV-2 main protease from a library of marine natural products: a virtual screening and molecular modeling study. *Mar Drugs* 18:225. <https://doi.org/10.3390/md18040225>
- Gupta RK (2021) Will SARS-CoV-2 variants of concern affect the promise of vaccines? *Nat Rev Immunol* 21:340–341. <https://doi.org/10.1038/s41577-021-00556-5>
- Gurung AB, Ali MA, Lee J, Farah MA, Al-Anazi KM (2020) Unravelling lead antiviral phytochemicals for the inhibition of SARS-CoV-2 Mpro enzyme through in silico approach. *Life Sci*. <https://doi.org/10.1016/j.lfs.2020.117831>
- Hemmati S, Behzadipour Y, Haddad M (2020) Decoding the proteome of severe acute respiratory syndrome coronavirus 2 (SARS-CoV-2) for cell-penetrating peptides involved in pathogenesis or applicable as drug delivery vectors. *Infect Genet Evol* 85:104474. <https://doi.org/10.1016/j.meegid.2020.104474>
- Hilgenfeld R (2014) From SARS to MERS: crystallographic studies on coronavirus proteases enable antiviral drug design. *FEBS J* 281:4085–4096. <https://doi.org/10.1111/febs.12936>
- Jin Z, Du X, Xu Y, Deng Y, Liu M, Zhao Y, Zhang B, Li X, Zhang L, Peng C, Duan Y, Yu J, Wang L, Yang K, Liu F, Jiang R, Yang X, You T, Liu X, Yang X, Bai F, Liu H, Liu X, Guddat LW, Xu W, Xiao G, Qin C, Shi Z, Jiang H, Rao Z, Yang H (2020) Structure of Mpro from SARS-CoV-2 and discovery of its inhibitors. *Nature* 582:289–293. <https://doi.org/10.1038/s41586-020-2223-y>
- Jukić M, Škrlj B, Tomšič G, Pleško S, Podlipnik Č, Bren U (2021) Prioritisation of compounds for 3CLpro inhibitor development on SARS-CoV-2 variants. *Molecules* 26:3003. <https://doi.org/10.3390/molecules26103003>
- Khateeb J, Li Y, Zhang H (2021) Emerging SARS-CoV-2 variants of concern and potential intervention approaches. *Crit Care* 25:244. <https://doi.org/10.1186/s13054-021-03662-x>
- Kim Y, Lovell S, Tiew K-C, Mandadapu SR, Alliston KR, Battaile KP, Groutas WC, Chang K-O (2012) Broad-spectrum antivirals against 3C or 3C-like proteases of picornaviruses, noroviruses, and coronaviruses. *J Virol* 86:11754–11762. <https://doi.org/10.1128/jvi.01348-12>
- Korhonen H (2009) Milk-derived bioactive peptides: from science to applications. *J Funct Foods* 1:177–187. <https://doi.org/10.1016/j.jff.2009.01.007>
- Kumari R, Kumar R, Consortium OSDD, Lynn A (2014) g_mmpbsa—A GROMACS tool for high-throughput MM-PBSA calculations. *J Chem Inf Model* 54:1951–1962. <https://doi.org/10.1021/ci50020m>
- Leach AG, Jones HD, Cosgrove DA, Kenny PW, Ruston L, MacFaul P, Wood JM, Colclough N, Law B (2006) Matched molecular pairs as a guide in the optimization of pharmaceutical properties; a study of aqueous solubility, plasma protein binding and oral exposure. *J Med Chem* 49:6672–6682. <https://doi.org/10.1021/jm0605233>
- Lipinski CA (2000) Drug-like properties and the causes of poor solubility and poor permeability. *J Pharmacol Toxicol Methods* 44:235–249. [https://doi.org/10.1016/s1056-8719\(00\)00107-6](https://doi.org/10.1016/s1056-8719(00)00107-6)
- Mimoto T, Hattori N, Takaku H, Kisanuki S, Fukazawa T, Terashima K, Kato R, Nojima S, Misawa S, Ueno T (2000) Structure-activity relationship of orally potent tripeptide-based HIV protease inhibitors containing hydroxymethylcarbonyl isostere. *Chem Pharm Bull* 48:1310–1326. <https://doi.org/10.1248/cpb.48.1310>
- Mohanty DP, Mohapatra S, Misra S, Sahu PS (2016) Milk derived bioactive peptides and their impact on human health – a review. *Saudi J Biol Sci* 23:577–583. <https://doi.org/10.1016/j.sjbs.2015.06.005>
- Moreno-Eutimio MA, López-Macías C, Pastelin-Palacios R (2020) Bioinformatic analysis and identification of single-stranded RNA sequences recognized by TLR7/8 in the SARS-CoV-2, SARS-CoV, and MERS-CoV genomes. *Microb Infect* 22:226–229. <https://doi.org/10.1016/j.micinf.2020.04.009>
- Pan Y, Lee A, Wan J, Coventry MJ, Michalski WP, Shiell B, Roginski H (2006) Antiviral properties of milk proteins and peptides. *Int Dairy J* 16:1252–1261. <https://doi.org/10.1016/j.idairyj.2006.06.010>

- Paniz-Mondolfi A, Bryce C, Grimes Z, Gordon RE, Reidy J, Lednický J, Sordillo EM, Fowkes M (2020) Central nervous system involvement by severe acute respiratory syndrome coronavirus-2 (SARS-CoV-2). *J Med Virol* 92:699–702. <https://doi.org/10.1002/jmv.25915>
- Panyayai T, Ngamphiw C, Tongsimma S, Mhuantong W, Limsripraphan W, Choowongkamon K, Sawatdichaikul O (2019) PeptideDB: a web application for new bioactive peptides from food protein. *Heliyon* 5:e02076. <https://doi.org/10.1016/j.heliyon.2019.e02076>
- Pillaiyar T, Meenakshisundaram S, Manickam M (2020) Recent discovery and development of inhibitors targeting coronaviruses. *Drug Discov Today* 25:668–688. <https://doi.org/10.1016/j.drudis.2020.01.015>
- Pirhadi S, Damghani T, Avestan MS, Sharifi S (2020) Dual potent c-Met and ALK inhibitors: from common feature pharmacophore modeling to structure based virtual screening. *J Recept Signal Transduct Res* 40:357–364. <https://doi.org/10.1080/10799893.2020.1735418>
- Planas D, Veyer D, Baidaliuk A, Staropoli I, Guivel-Benhassine F, Rajah MM, Planchais C, Porrot F, Robillard N, Puech J, Prot M, Gallais F, Gantner P, Velay A, Le Guen J, Kassis-Chikhani N, Edriss D, Belec L, Seve A, Courtellemont L, Péré H, Hocqueloux L, Fafi-Kremer S, Prazuck T, Mouquet H, Bruel T, Simon-Lorière E, Rey FA, Schwartz O (2021) Reduced sensitivity of SARS-CoV-2 variant Delta to antibody neutralization. *Nature* 596:276–280. <https://doi.org/10.1038/s41586-021-03777-9>
- Pradeep H, Najma U, Aparna HS (2021) Milk peptides as novel multi-targeted therapeutic candidates for SARS-CoV2. *Protein J* 40:310–327. <https://doi.org/10.1007/s10930-021-09983-8>
- Prudhomme M (2013) *Advances in anticancer agents in medicinal chemistry*. Bentham Science Publishers, Sharjah
- Rahmatabadi SS, Sadeghian I, Ghasemi Y, Sakhteman A, Hemmati S (2019) Identification and characterization of a sterically robust phenylalanine ammonia-lyase among 481 natural isoforms through association of in silico and in vitro studies. *Enzyme Microb Technol* 122:36–54. <https://doi.org/10.1016/j.enzmictec.2018.12.006>
- Randolph JT, Zhang X, Huang PP, Klein LL, Kurtz KA, Konstantinidis AK, He W, Kati WM, Kempf DJ (2008) Synthesis, antiviral activity, and conformational studies of a P3 aza-peptide analog of a potent macrocyclic tripeptide HCV protease inhibitor. *Biorganic Med Chem Lett* 18:2745–2750. <https://doi.org/10.1016/j.bmcl.2008.02.053>
- Rubio-Aliaga I, Daniel H (2008) Peptide transporters and their roles in physiological processes and drug disposition. *Xenobiotica* 38:1022–1042. <https://doi.org/10.1080/00498250701875254>
- Santos S, Torcato I, Castanho MA (2012) Biomedical applications of dipeptides and tripeptides. *Pept Sci* 98:288–293. <https://doi.org/10.1002/bip.22067>
- Schüller A, Yin Z, Brian Chia CS, Doan DNP, Kim H-K, Shang L, Loh TP, Hill J, Vasudevan SG (2011) Tripeptide inhibitors of dengue and West Nile virus NS2B–NS3 protease. *Antiviral Res* 92:96–101. <https://doi.org/10.1016/j.antiviral.2011.07.002>
- Shankar G, Arkin S, Cocea L, Devanarayan V, Kirshner S, Kromminga A, Quarmby V, Richards S, Schneider CK, Subramanyam M, Swanson S, Verthelyi D, Yim S (2014) Assessment and reporting of the clinical immunogenicity of therapeutic proteins and peptides-harmonized terminology and tactical recommendations. *AAPS J* 16:658–673. <https://doi.org/10.1208/s12248-014-9599-2>
- Sharma P, Kaur H, Kehinde BA, Chhikara N, Sharma D, Panghal A (2021) Food-derived anticancer peptides: a review. *Int J Pept Res Ther* 27:55–70. <https://doi.org/10.1007/s10989-020-10063-1>
- Win TS, Malik AA, Prachayasittikul V, Wikberg S, Nantasenamat JE, Shoombuatong C (2017) HemoPred: a web server for predicting the hemolytic activity of peptides. *Future Med Chem* 9:275–291. <https://doi.org/10.4155/fmc-2016-0188>
- Xu Q, Hong H, Wu J, Yan X (2019a) Bioavailability of bioactive peptides derived from food proteins across the intestinal epithelial membrane: a review. *Trends Food Sci Technol* 86:399–411. <https://doi.org/10.1016/j.tifs.2019.02.050>
- Xu Q, Yan X, Zhang Y, Wu J (2019b) Current understanding of transport and bioavailability of bioactive peptides derived from dairy proteins: a review. *Int J Food Sci Technol* 54:1930–1941. <https://doi.org/10.1111/ijfs.14055>
- Yang H, Yang M, Ding Y, Liu Y, Lou Z, Zhou Z, Sun L, Mo L, Ye S, Pang H, Gao GF, Anand K, Bartlam M, Hilgenfeld R, Rao Z (2003) The crystal structures of severe acute respiratory syndrome virus main protease and its complex with an inhibitor. *Proc Natl Acad Sci U S A* 100:13190–13195. <https://doi.org/10.1073/pnas.1835675100>
- Yang H, Lou C, Sun L, Li J, Cai Y, Wang Z, Li W, Liu G, Tang Y (2019) admetSAR 2.0: web-service for prediction and optimization of chemical ADMET properties. *Bioinformatics* 35:1067–1069. <https://doi.org/10.1093/bioinformatics/bty707>
- Zhang L, Lin D, Sun X, Curth U, Drosten C, Sauerhering L, Becker S, Rox K, Hilgenfeld R (2020) Crystal structure of SARS-CoV-2 main protease provides a basis for design of improved α -ketoamide inhibitors. *Science* 368:409–412. <https://doi.org/10.1126/science.abb3405>

Publisher's Note Springer Nature remains neutral with regard to jurisdictional claims in published maps and institutional affiliations.